Landmine detection: on the imaging capabilities of γ-ray Compton backscattering

M.L. Cortés,[1] E. Merchán,[1] W.J. Blanco,[1] F. Cristancho,[1] J. Gerl,[2] and F. Ameil[2]

[1]Universidad Nacional de Colombia, Bogotá, Colombia; Centro Internacional de Física, Bogotá, Colombia
[2]Gesellschaft für Schwerionenforschung, Darmstadt, Germany
(Dated: May 23, 2008)

Two issues related with the use of γ-ray Compton backscattering as an imaging technique are addressed: γ-soil interaction, and image processing. Promising methodologies are described in both topics.

I. INTRODUCTION

The use of the γ-ray Compton backscattering as the main tool to construct an imaging system able of identifying landmines buried in soil has proven very promising in its first prototype developments [1, 2]. These prototypes take advantage of the back-to-back positronic 511 keV annihilation. One of the γ-rays is used to tag the backscattering signal from the other one.

By sampling coincidence events an image is built reflecting mainly the distribution of the electron density of the matter placed in front of the prototype device. Laboratory and field tests have shown that although an image of enough quality to guess the presence of objects buried into the soil is achieved, closer characterization of the potential mine is hampered by difficulties related to our rather poor knowledge of two main processes: (*i*) the γ-soil interaction, and (*ii*) the effects that the different hardware pieces and software procedures have on the final image.

II. STUDY OF THE γ-SOIL INTERACTION

Regarding the first point of previous section, the problem is that although the Klein-Nishina cross-section predicts exactly the result of a one-step γ-electron interaction, the result of such a complex process as a multi-step collision of a γ-ray with a target as intricate as the multi-element, macroscopic soil is very difficult to predict.

The experiments explained below are motivated by following reasoning: if one places a mono-energetic gamma source in front of a gamma detector in vacuum, that is, there is no material between source and detector, the recorded spectrum contains two parts: a Gaussian peak associated to complete absorption of the photon by the detector, and a region originated by the Compton effect taking place in the detector itself. This part of the spectrum extends between 0 keV and a value called Compton border (341 keV for a 511 keV photon). Actually multi-Compton events will extend such region beyond the Compton border. The number of counts and its spectral distribution within each of the two regions are characteristic of the γ-detector interaction. If one places some material between source and detector, the previous simple picture will be modified. Those modifications can be summarized as:

1. Intensity and distribution of the Compton region will change because the photons reaching the detector will not be mono-energetic anymore.
2. Related with the previous point, the region between the Compton border and the photopeak will be filled because the photons have the chance to scatter at low-angles in the soil and then be absorbed in the detector.
3. The intensity in the Gaussian peak will decrease as a result of the attenuation of the beam.

Figure 1 gives schematically the experimental elements discussed above. The NaI and Ge detectors are connected in time-coincidence. In this way one of the 511 keV γ-rays, produced after positronic emission of the ^{22}Na source, will be detected by the NaI detector, whereas the other γ-ray will have the chance of interacting with the soil and then be absorbed by the Ge detector.

Figure 2 displays a GEANT4 [3] simulated Ge spectrum. The spectra are normalized to the height of the photopeak to magnify the effects. As discussed above the placement of thicker layers of soil between source and detector modifies the spectral shape. Of main interest is the observation of the filling of the region $E_\gamma > 400$ keV. We
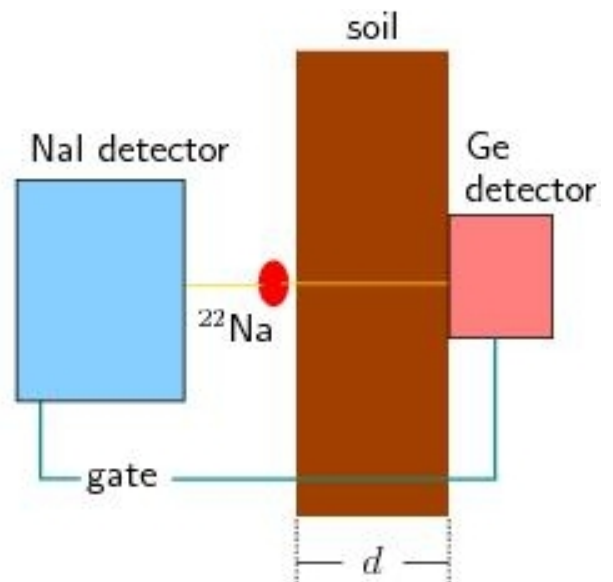

FIG. 1: Experimental set-up used to perform experiments on transmission of γ-rays in soil.
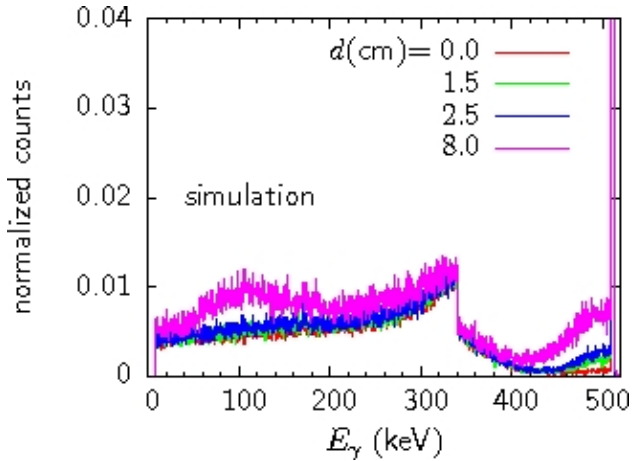
FIG. 2: GEANT4 simulations of the spectra detected with the Ge in coincidence with the NaI detector in the geometrical array shown in Fig. 1.

observe that the effect increases for thicker layers of soil. Another important effect is observed: for thicker soil a "bump" is formed around 100 keV originating in an increased probability for multiple Compton scattering. All of these effects are in agreement with the three points listed above. At this stage of the work, although the simulation contains the essential characteristics of the experiment (geometry, dimensions, main components), it is still rather schematic, missing several details (containers of crystals and soil, for example). Because of this reason we use the simulation only to obtain a gross prediction of the experimental results.

Figure 3 shows experimental spectra obtained with three different thicknesses of soil. As explained above, we did not try to match exactly the simulated parameters. Even so the expected behavior of the simulation in Fig. 2 is in fact regained experimentally.
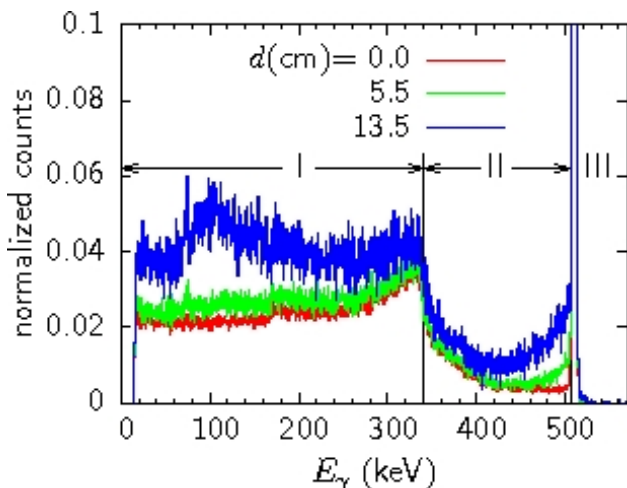

FIG. 3: Experimental spectra (normalized to the photopeak height) for three different values of soil thickness.
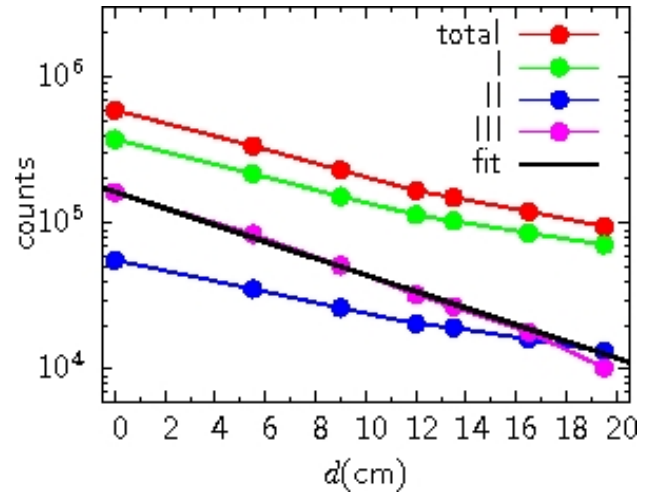

FIG. 4: Number of counts in the Ge detector as a function of thickness of the soil layer for the three different regions of the spectrum depicted in (a): I) Compton region: 0–341 keV; II) Valley: 341–506 keV; III) Photopeak at 511 keV.

In order to evaluate the effect of the soil thickness on detected spectra, we define three regions in the spectra according to the three types of modifications listed above and depicted with the same labeling in Fig. 3: I) Compton region: $0 - 341$ keV; II) Valley: $341 - 506$ keV; III) Photopeak at 511 keV.

Figure 4 displays the dependence of the intensity in each region as a function of d. Three main observations are gained:

1. An approximate exponential dependence is observed for each one of the data sets. The slope, however, is similar for the regions I (Compton region) and II (valley) and different at any d value of the region III (photopeak).

2. At $d \approx 12$ cm a change of slope takes place for all but the photopeak data.

3. The photopeak data have been fitted to an exponential function $I(d) = I_0 \exp(-\mu\, d)$ resulting in $\mu = 0.131(3)$ cm^{-1} in agreement within 1.5% of the reported value for dry sand (SiO_2) in standard reference databases [4]. Additional experiments with different types of soil should clarify whether the slope similarities and differences (previous point 1 and the slope change at $d \approx 12$ cm are meaningful features.

III. IMAGE PROCESSING

Ongoing work [1, 2] has proven the capability that a Compton backscattering imaging device has to identify objects buried in soil some centimeters in depth. Such identification takes place by visualizing the buried object. Top of Fig. 5 shows the image of a lead disk 5 cm in radius placed on the surface of dry sand. One of the questions to
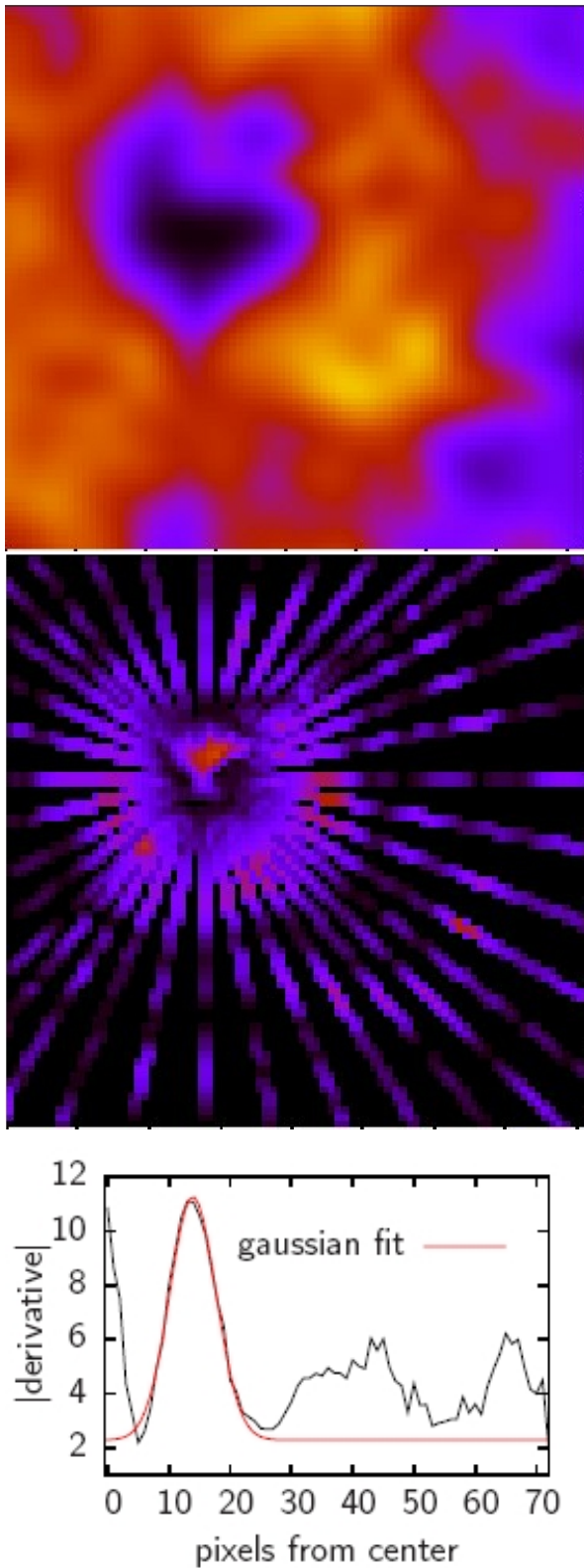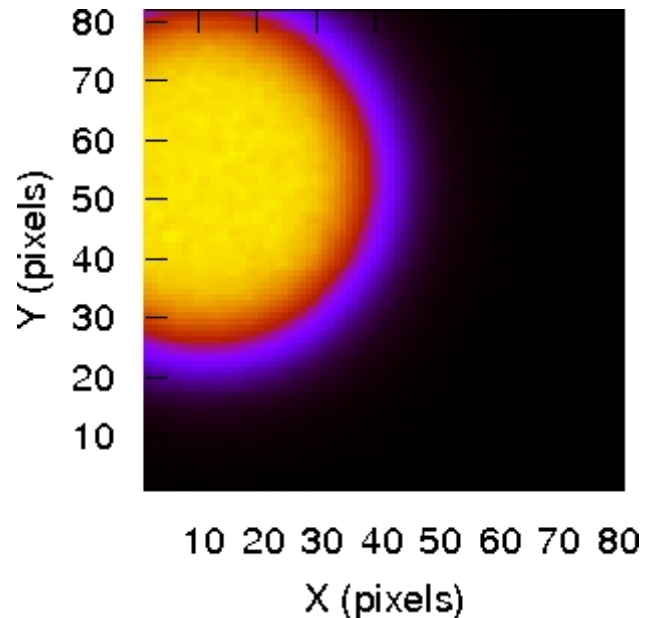
FIG. 6: Simulated image of a disk partially out of the view of field.

be answered when addressing the issue of identification is how to estimate the size of the investigated object. The first part of that task is called "edge detection". We have defined following procedure:

1. Assume that the projected shape is circular.
2. Select (by hand or by code) a "center" from which "rays" are traced.
3. Find the derivative as a function of the distance from the center.
4. Add the absolute values of the derivative for the pixels at the same distance from the center (circular projection).

The result is a bi-dimensional histogram. The coordinate of its maximum corresponds to the border of the object. Figure 5 (middle) illustrates such a procedure with the lead plate image when only 36 rays are traced. Values of the derivative histogram are shown in Fig. 5 (bottom) from which we conclude that the radius is 14(4) pixels. Additional trigonometrical considerations allow us to evaluate the physical radius in centimeters.

Working with experimentally obtained images offers one major difficulty related with the fact that it is not possible to check the quality of the used software. In order to perform this check, we decided to numerically simulate images in which the size parameters and even the quality is adjustable. We simulate circular shapes by randomly selecting events from a Fermi-Dirac two-dimensional probability density distribution

$$f(r) = \frac{1}{1 + \exp[(r - r_0)/a]} \qquad r = \sqrt{x^2 + y^2}, \quad (1)$$

FIG. 5: (top) Image of a lead disk. (middle) Map of derivatives. Only data along the rays are represented. The rest of the surface is black. (bottom) Circular projection of the derivative according to the procedure explained in the text.

being (x, y) the Cartesian coordinates of a given pixel. The usefulness of this kind of distribution lies in the fact that the radius of the object's image, r_0, and its "fuzziness" in the picture, a, can be mathematically parametrized. For a given image dimension (84 pixels × 84 pixels in this work), its quality is decided by the number of simulated histories.

Figure 6 shows one of such images. The disk has been purposely placed partially out of the field of view in order to magnify some of the problems found in our procedure: i) Deep valleys connecting the center of the figure and the corners of the picture appear in the derivative map shown in top of Fig. 7. These valleys are an artifact of the procedure originated in the fact that in order to properly analyze the plane, 4 sectors have to be defined. The borders of the sectors offer continuity problems that translate visually into these valleys. ii) Figure 7 (bot-

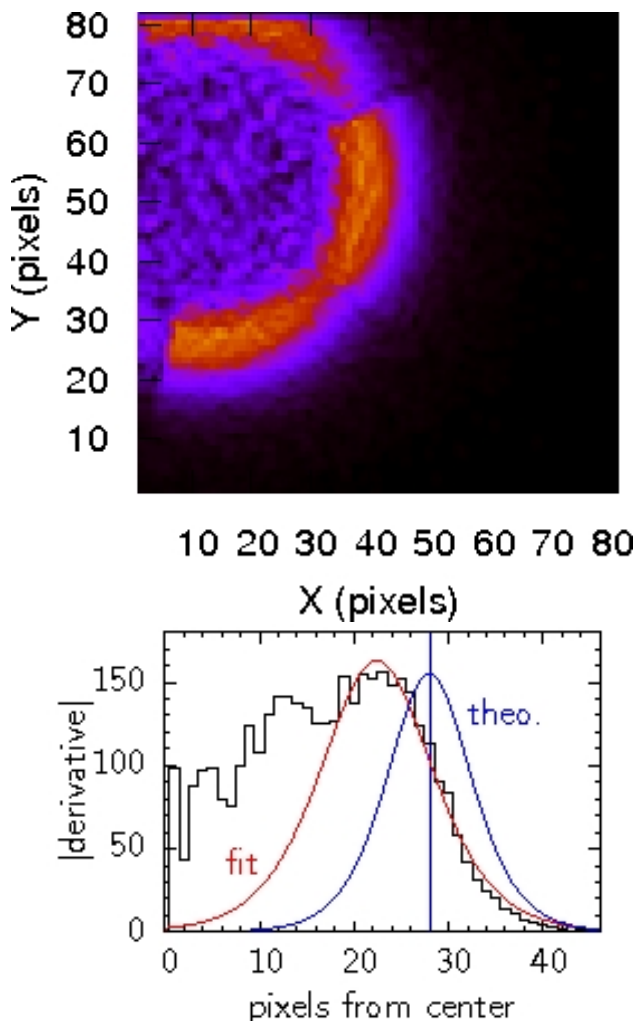FIG. 8: Map of the gradient of the image shown in Fig. 6. Compare with Fig. 7.

FIG. 7: Map of derivatives (top) and Circular projection of the derivative's absolute value. The same Eq. (1) is used for both curves. The fit does not reproduce the theoretical parameters.
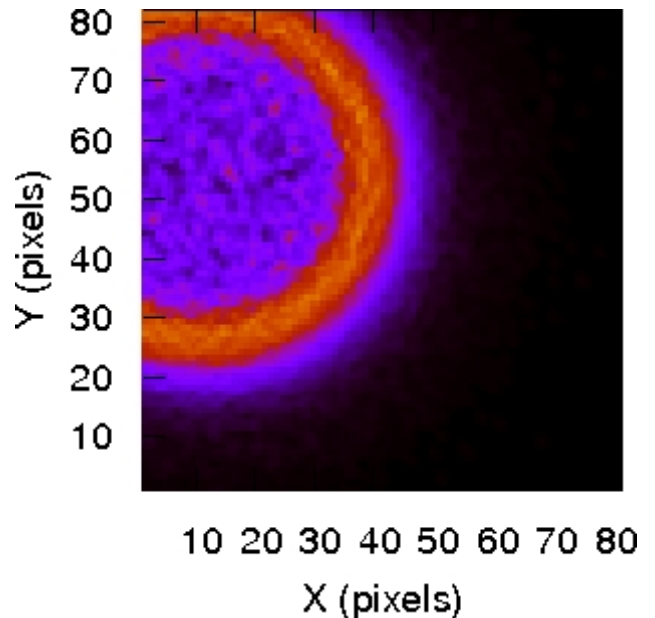
tom) gives the resulting histogram. If the algorithm could correctly predict the position of the border, the blue curve (the derivative of the simulated probability function) would be the resulting fit. We see that the algorithm erroneously overestimates the derivative values in the region $0 - 15$ pixels, producing an underestimation of the radius: the fitted derivative predicts $r = 22$ pixels, whereas the simulated one has $r = 28$ pixels.

In order to solve the listed problems we have tried a different approach. Instead of calculating the derivatives along a given straight line (rays) we evaluate its generalization, the gradient of the 3-dimensional image. Fig. 8 shows the resulting gradient map for the case of the disk already shown in Fig. 6. Clearly the gradient offers a high quality definition of the image maxima, and because the gradient is locally defined we do not stumble on the problem related with the sector borders.

IV. SUMMARY

We have addressed two issues related with the use of γ-ray Compton backscattering as an imaging technique: first, the complexity of the γ-soil interaction, and second, the possibility of processing so obtained images in order to identify physical parameters of the visualized objects. Regarding the first issue, we have shown that carefully planned experiments, helped by high-standards simulations can offer a way towards the understanding of the γ-soil interaction. Regarding image processing we have shown that there exist procedures that can help to improve our capability to interpret the images obtained with a γ-ray backscattering imaging device. The

progress reached in both issues simultaneously shows that improved experimentation and the use of more sophisti-

cated mathematical algorithms are needed.

[1] IAEA Technical Meeting on Combined Devices for Humanitarian Demining and Explosives Detection, 13-17 November 2006, INFN, Padova, Italy; see **STI/Pub/1300** (2007) ISBN 978-92-0-157007-9.

[2] J. Gerl, Nucl. Phys. **A752**, 688c (2005).

[3] S. Agostinelli *et al.*, Nucl. Inst. Meth. Phys. Res. A **506**, 250 (2003).

[4] Photopeak for dry sand